The Astrophysical Journal Letters, 975:L39 (6pp), 2024 November 10 https://doi.org/10.3847/2041-8213/ad85e1

Overestimation of Astrophysical Gamma-Ray Energies during Thunderstorms: Synergy of Galactic and Atmospheric Accelerators

A. Chilingarian and M. Zazyan
Yerevan Physics Institute, Alikhanyan Brothers 2, Yerevan, AM0036, Armenia
Received 2024 September 8; revised 2024 October 6; accepted 2024 October 8; published 2024 November 6

Abstract

Particle accelerators abound in space plasmas, saturating the cosmos with fully stripped nuclei and gamma rays, with energies surpassing the capabilities of human-made accelerators by orders of magnitude. Upon reaching Earth's atmosphere, these particles trigger extensive air showers (EASs), generating millions of secondary cosmic rays of lower energies. Free electrons from EASs developing in the atmosphere are seeds for atmospheric electron accelerators. Strong atmospheric electric fields (AEFs) evolving during thunderstorms act as accelerators, amplifying the intensity of electrons many times, significantly enlarging the EAS size (number of electrons). Thus, the energy of the primary cosmic ray recovered by EAS size can be significantly overestimated. Recently discovered by high-altitude EAS arrays, PeVatron candidates (ultra–high-energy (UHE) astrophysical gamma-ray sources) must be carefully examined according to the atmospheric conditions during EAS detection. Large High Altitude Air Shower Observatory and High-Altitude Water Cherenkov Observatory arrays are located in regions of frequent thunderstorms, and an AEF's strength can reach and surpass the critical strength to start relativistic runaway electron avalanches. A few registered UHE gamma rays from stellar sources can be registered at just this time when the AEF highly enhances the EAS size. Thunderstorm ground enhancements are copiously registered at mountain peaks of Eastern Europe, Germany, and Armenia, with energies well above the threshold energy of EAS array scintillators. Thus, the overestimation of the energy of primary particles is not an exotic process but a consequence of already well-established physical phenomena. Consequently, a report on each registered UHE gamma ray should include the recorded time and corresponding weather conditions.

Unified Astronomy Thesaurus concepts: Galactic cosmic rays (567)

1. Introduction

Very high-energy (VHE; 0.1–100 TeV) and ultra–high-energy (UHE; >100 TeV) gamma-rays open a new window to the Universe. The major motivation of gamma-ray astronomy is to find galactic sources of cosmic rays, such as pulsars, pulsar wind nebulae, supernova remnants (SNRs), binary systems, and clusters of young stars. Galactic magnetic fields confine these particles, keeping them within the Milky Way for long periods. This confinement increases the probability of cosmic rays being detected on Earth before escaping into intergalactic space. In the solar system, charged particles arrive highly isotropically and enter the terrestrial atmosphere with energies above the cutoff rigidity ranging from 0.3 to 17 GeV, dependent on geographical coordinates and entrance angles. In the terrestrial atmosphere, they unleash extensive air showers (EASs), which reach the ground and are registered by distributed networks of particle detectors. Integrating the measured density of particles, the number of electrons (EAS size) and muons were recovered to estimate the primary particle energy. Additional triggers can outline electromagnetic EASs initiated by gamma rays (muon-poor EASs). This option, adding the high location of the detector, is especially important for establishing UHE gamma-ray astronomy. Different classification schemes have been developed to analyze multivariate EAS data and differentiate EASs initiated by various types of primary particles. The energy spectrum of light nuclei was measured by the MAKET-ANI detector (A. Chilingarian et al. 2004), located at 3200 m (40°25N, 44° 15E). The compact array consisted of nearly 100 plastic scintillators that selected showers from $\approx$1000 m^2 with an efficiency of more than 95% (see details in A. Chilingarian et al. 2007). The data analysis scheme uses nonparametric multivariate methods (A. A. Chilingarian 1989) and Bayesian and neural network techniques (see details in T. Antoni et al. 2002). In this way event-by-event classification of EAS (A. Chilingarian & H. Zazyan 1991) was checked by both methods and under alternative models of strong interaction models.

An approach for preparing enriched cosmic-ray mass groups was used in the KASCADE experiment (T. Antoni et al. 2003a). For preparing samples enriched with events of light, intermittent, and heavy mass groups, the (N_e, N_μ) correlation has been exploited as a mass identifier, using reference patterns from Monte Carlo simulations (T. Antoni et al. 2003b). Atmospheric Cherenkov telescopes also present results on the proton energy spectrum; see, for instance, F. Aharonian et al. (1999). Different experimental techniques for obtaining the proton energy spectrum give rather consistent results, as shown in G. Hovsepyan & A. Chilingarian (2023).

Recently published by the Large High Altitude Air Shower Observatory (LHAASO), all-particle energy spectra (Z. Cao et al. 2024a) precisely coincide with MAKET-ANI results on spectral indices before and after the knee (G. V. Kulikov & G. B. Christiansen 1958). Unfortunately, the LHAASO collaboration does not implement the particle classification scheme. It does not present the light nuclei energy spectrum, instead discussing the energy dependence of the mean

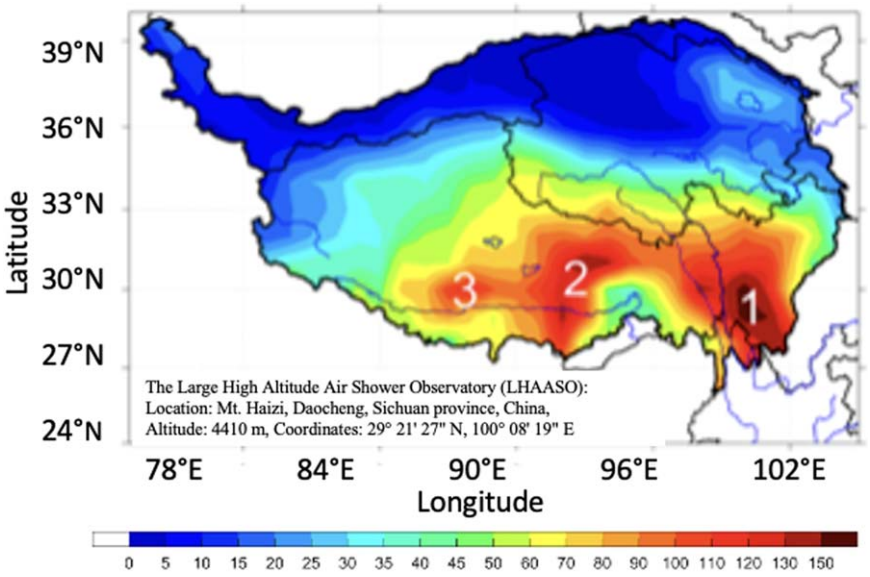

Figure 1. Spatial distribution of thunderstorm activity. The grid is $1^\circ \times 1^\circ$ (equivalent to a circle with a radius of 48 km), and the color coded values indicate the average annual THN. Adopted from Y. Du et al. (2022).

logarithm mass of cosmic rays. In contrast, the MAKET-ANI and KASCADE present the energy spectra of light and heavy nuclei separately. The main experimental results on energy spectra provide evidence of the rigidity-dependent acceleration at the outer boundaries of SNRs (A. Chilingarian et al. 2007). The estimated energy spectrum of the light mass group of nuclei shows a very sharp knee at $\approx$2.8 PeV: $\Delta \approx 0.9$, compared to $\Delta \approx 0.4$ for the all-particle energy spectra. The energy spectrum of the heavy mass group of cosmic rays shows no knee in the 10^{15}–2×10^{16} eV energy range. Theoretical models suggest that SNRs within our Galaxy can accelerate particles to 100 TeV, and acceleration is rigidity dependent, i.e., protons escape from the SNR magnetic traps first and heavy nuclei, later ascending more energies. The "knee" feature at $\approx$3 PeV suggested that protons can be accelerated to such energies, and gamma rays born in the p–p interactions can reach energies of 300 TeV. Observations of UHE gamma rays allow the PeV proton interaction to be directly probed. Therefore, registration of the UHE gamma rays from the SNR and other galactic objects will be key evidence for the CR origin and will establish gamma-ray astronomy for revealing galactic accelerators.

The following observatories are looking for PeVatrons:

LHAASO (Figure 1) is located at Mt. Haizi (4410 m a.s.l., 600 g cm^{-2}, 29°21′27.″56N, 100°08′19.″66E) in Daocheng, Sichuan province, P.R. China.

YangBaJing Cosmic Ray Observatory (ASγ Collaboration, Tibet, P.R. China, 4300 m a.s.l., 606 g cm^{-2}, 90.°5 East, 30.°1 North).

High-Altitude Water Cherenkov Observatory (HAWC) is located at Sierra Negra (4100 m a.s.l., 745 g cm^{-2}, 18°59.′7N, 97°18.′5W) in Puebla, Mexico.

A series of papers from these observatories have already published several PeVatron candidates, claiming the registration of galactic sources. The first detection of UHE photons from an astrophysical source (Crab Nebula) was reported by the Tibet ASγ Collaboration (M. Amenomori et al. 2019). The estimated energies of 24 photon-like events exceed 100 TeV and 4–250 TeV.

HAWC observatory reported the detection of nearly 100 gamma rays from the Galactic center with energies above 100 TeV (A. Albert et al. 2024). The measured gamma-ray luminosity suggests the presence of PeVatrons in the Galactic center.

The LHAASO observatory presents the catalog of 90 VHE and UHE source candidates compiled using 508 days of data collected by the Water Cherenkov Detector Array from 2021 March to 2022 September and 933 days of data recorded by the Kilometer Squared Array from 2020 January to 2022 September (Z. Cao et al. 2024b). Gamma rays from 43 sources have energies above 100 TeV.

Thus, the new-generation arrays revive interest in the "knee" region physics and prove that they can extend the observation to the UHE range due to their large area, diversity of particle detectors, and long duty cycle. However, all three observatories are in mountain regions, where thunderstorms are frequent, and strong electric fields are expected. Therefore, there is a possibility of overestimating gamma-ray energy due to the multiplication of EAS electrons in strong atmospheric electric fields (AEFs) emerging above detectors. Taking the LHAASO observatory as an example, we will describe the site's climatology and model the propagation of EASs initiated by gamma rays of various energies in the terrestrial atmosphere until they reach the detector. Possible energy overestimation will be accessed and discussed.

2. LHAASO Site Climatology

The technique of recovering energy and type of primary nuclei includes sophisticated statistical analysis schemes of copious secondary particles born in the atmosphere. The strong interaction models, air density, and geomagnetic field were incorporated into the models of shower development. However, the influence of the AEFs emerging in thunderous atmospheres was not accounted for until recently. However, it was shown by A. Chilingarian et al. (2022) that an electric field above the LHAASO observatory can lead to a large overestimation of the primary gamma-ray energy. Therefore, it is crucial to include in procedures of energy estimation a careful account of climatic

conditions. Unfortunately, the near-surface electric field measurements (a proxy of the AEF) are not presented in the catalog of PeVatrons published by LHAASO (Cao et al. 2024b).

Furthermore, the date and time of VHE and UHE energy gamma rays were not included. The time and date can be neglected if there are large amounts of the highest-energy gamma rays. However, for the unique measurements of PeVatrons, usually limited by 1–2 UHE gamma rays, detailed information on the date, time, and climatic parameters is necessary.

The Tibetan Plateau experiences unique lightning activity due to its high altitude and specific climatic conditions. The Qinghai–Tibet Plateau (QTP) is important for its significant effects on the global weather system due to its extensive area, spanning approximately 2800 km from east to west and 1500 km from north to south, and high terrain (with an average altitude of more than 4000 m). This region has long been a subject of interest for meteorologists (T. Zou et al. 2018; J. Zhu et al. 2023). In the study of Y. Du et al. (2022), the annual thunderstorm hour number (THN) was recovered above the QTP from the thunderstorm cloud data set from the geostationary FY-2E satellite (R. Ma et al. 2021) and the Worldwide Lightning Location Network (WWLLN; P. Fan et al. 2018). The lightning data were used to identify the thunderstorm, and the satellite observation provided information on the cloud's location and size. The satellite observation is important because WWLLN tends to detect stronger cloud-to-ground (−CG) lightning flashes, and the detection efficiency of most frequent intracloud flashes (+IC and—IC) is only ≈10%.

Figure 1 shows the spatial distribution of thunderstorm activity over the QTP. An active thunderstorm belt extended westward from 101°E to 86°E, including three high-density southeast centers. The first and most intense one includes the LHAASO observatory (TNH ≈ 150), and the third includes the YangBaJing Cosmic Ray Observatory (TNH ≈ 100). The mean TNH over the QTP is ≈80. Climate change has led to more frequent and intense convective activities in the region, increasing the AEF during storm events.

Around 94% of thunderstorms over the QTP occur from May to September and from 12:00 to 21:00 local time, as shown in Figure 4 of Y. Du et al. (2022). From remote sensing, the average area of thunderstorm clouds was estimated to be approximately 2×10^4 km^2. The spatial distribution of thunderstorm vertical development height relative to the surface aligns with the horizontal extension, indicating stronger convection in the eastern QTP. The thunderstorm charge structure has long been a major topic in atmospheric physics. A tripole structure, as proposed by J. Kuettner (1950), has been well accepted for decades. However, the charge structure of a storm is dynamically developed and can be more complex. X. Qie et al. (2009) divided thunderstorms over the QTP into two categories: one with a large positively charged lower region at the base of the thundercloud and one without it. Two dipoles emerge between the main negatively charged region (MN) and LPCR and between MN and its mirror in the Earth, accelerating electrons downward (A. Chilingarian & H. Mkrtchyan 2012). If the electric field strength surpasses the critical value specific for air density, a relativistic runaway electron avalanche (RREA; A. V. Gurevich et al. 1992) is unleashed, covering large areas beneath with enhanced fluxes of electrons, positrons, gamma rays, and rare neutrons (A. Chilingarian et al. 2010, 2024). The negative charge center is between 5.7 and 7.7 km above sea level, providing enough avalanche elongation path; the emerged large LPCR (D. Liu et al. 2024) indicates a low location of AEF above detectors. This leads to a short free-path distance (FPD; A. Chilingarian et al. 2024; E. Williams et al. 2023), the distance crossed by particles in the air after exiting from the AEF.

3. Effects of Thunderstorms' Electric Field on the EAS Electron Number (EAS Size)

All three experiments performed modeling of the EAS particle propagation in the thundercloud's electric fields above detectors (see the review by A. Chilingarian et al. 2024). However, the LHAASO experiment only recently examined the strong AEF's influence on EAS size and radial distribution. X.-X. Axikegu et al. (2024) demonstrate an increase of positron and electron number by 65% in a –1000 V cm^{-1} electric field and 992% in a –1700 V cm^{-1} field. It is mentioned that modeling can provide information on the acceleration and multiplication of the EAS particles caused by an AEF. C. Lin et al. (2024) added a uniform electric field of the same strength within the altitude of 4400–5400 m, obtaining an increase in the mean lateral radius of the secondary particles of about 9.9% and 119.0% at the primary energy of about 180 GeV and 560 TeV, respectively. The drastic increase in EAS lateral radius also led to a significant increase in shower size and, therefore, in the estimate of the primary gamma-ray energy.

Proceeding from our pilot study of energy overestimation (A. Chilingarian et al. 2022), we perform a study of EAS propagation through AEF above the LHAASO detector. We tested different primary gamma-ray energies (from 1 to 100 TeV), AEF strengths (1.7–1.9 kV cm^{-1}), and FPD (50–200 m).

COsmic Ray SImulations for KAscade (CORSIKA; D. Heck et al. 1998) is a detailed Monte Carlo program that models the propagation of almost all species of EASs in the atmosphere. It was developed primarily for the KASCADE experiment (T. Antoni et al. 2003a) at Karlsruhe. Afterward, CORSIKA became a benchmark for analyzing and comparing various experiments and strong interaction models. The latest version of CORSIKA, 7.7550 (D. Heck & T. Pierog 2024), was issued on 2024 April 30. CORSIKA provides the quantity, energy, coordinates, and angles of incidence of secondary leptons and hadrons at arbitrary atmospheric levels and Earth's surface for the incident hadrons with energies up to 1000 PeV distributed according to assumed energy spectra or for the fixed energies. Among several particle interaction models available for CORSIKA users, we select the GGSJET model (N. N. Kalmykov et al. 1997) for high-energy hadronic interactions, the UrQMD model (S. Bass 1998) for low energies, and the EGS4 (W. R. Nelson et al. 1985) model for electromagnetic interactions.

The latest CORSIKA versions include acceleration and multiplication processes emerging when charged particles enter AEF, which can be introduced at arbitrary altitudes. Primary gamma rays of fixed energies enter the atmosphere vertically, and all secondary particles were followed from the first interaction in the atmosphere to 4410 m height (LHAASO location). The AEF of 1.7–1.9 kV m^{-1} was introduced at 4460–6460 m heights. After entering the AEF, the RREA process accelerates secondary charged particles and unleashes electron–gamma-ray avalanches. The AEF terminated at 200,

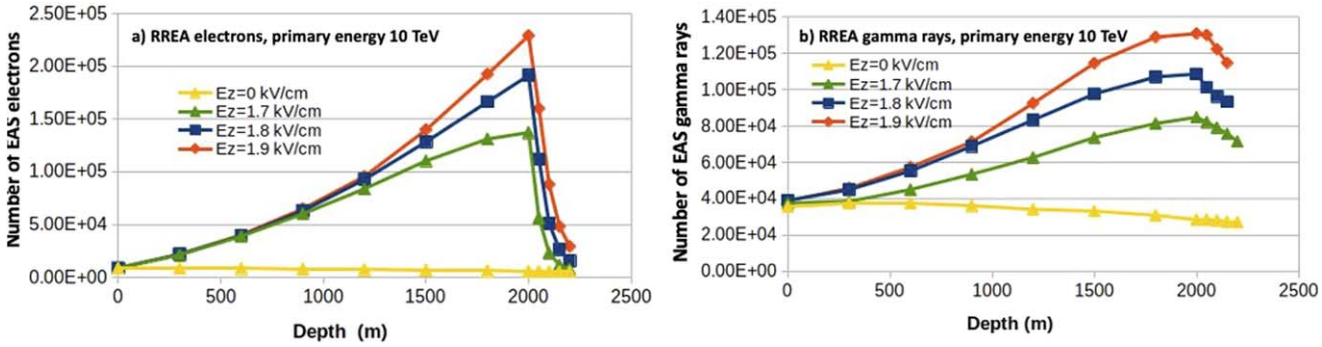

Figure 2. Propagation of the EAS in AEFs of different strengths: (a) electrons, (b) gamma rays. The number of particles is calculated at each 300 m in the AEF and each 50 m after exiting it at 200 m above detectors.

Table 1
Simulated Number of the EAS Particles at Fair Weather (Second Column) and after Crossing the Electric Field of Various Strengths (Particle Energy >3 MeV)

E_o (TeV)	$Ez = 0$ kV cm^{-1}		$Ez = 1.7$ kV cm^{-1}		$Ez = 1.8$ kV cm^{-1}		$Ez = 1.9$ kV cm^{-1}	
	N_γ	N_e	N_γ	N_e	N_γ	N_e	N_γ	N_e
1	1714	295	5791	9318	7575	14,455	10,138	19,099
10	27,515	5415	77,720	117,617	99,512	180,088	122,033	221,154
50	158,352	33,606	407,506	580,064	488,922	844,690	634,841	1,119,967
100	329,839	71,784	831,636	1,147,274	947,520	1,563,007	1,247,420	2,160,824

Table 2
The Estimates of Energy of the Primary Gamma Rays Obtained by Equation (1) with Ne Values from Table 1

E_o (TeV)	Estimates			
	$Ez = 0$ kV cm^{-1}	$Ez = 1.7$ kV cm^{-1}	$Ez = 1.8$ kV cm^{-1}	$Ez = 1.9$ kV cm^{-1}
1	0.96	9.22	16.65	22.63
10	10.89	75.85	136.05	184.21
50	50.48	300.88	496.31	713.01
100	94.83	502.21	838.46	1145.47

Note. The particles exit the AEF at 50 m above the detector.

150, 100, and 50 m above the ground. In this way, we tested the influence of the AEF height on the boost of EAS particles. The secondary electrons and gamma rays were followed and stored until energies reached 3 MeV. The number of particles was calculated for each 300 m in AEF and each 50 m after exiting it. See an example of the input parameters file in the supplementary materials.

In Figure 2, we show the significant enhancement of the EAS electrons and gamma rays after crossing 2 km AEF for the primary gamma ray with energy 10 TeV. For the electric field of 1.7 kV m^{-1}, shower size exceeds 10^5 (green curve; without AEF, it should be only 295; see Table 1); for AEF, 1.9 kV m^{-1}, it exceeds 2×10^5 (red curve). Within the AEF, the number of electrons always exceeds the number of gamma rays. However, after exiting from the AEF, the number of electrons strictly diminished due to ionization losses, and after 50 m propagating in the air, the number of gamma rays exceeded the number of electrons. No electron reaches the ground if it exits AEF at 200 m.

Table 1 presents the simulation results for different AEF strengths and primary gamma-ray energies. The EAS leaves the AEF 50 m above the LHAASO detector. We chose an FDP equal to 50 m, according to the data from the largest thunderstorm ground enhancements registered on Mount Aragats in 2023 (height 3200 m; A. Chilingarian et al. 2024).

The fair-weather values from Table 1 were used to make an energy estimator by fitting the regression coefficient of the primary energy (E_0,TeV) and shower size (N_e) relation, which was used as the primary energy estimator:

$$\mathrm{Log}_{10}E_0 = 0.85\mathrm{Log}_{10}N_e - 2.1. \quad (1)$$

The regression coefficient obtained agrees with world data (S. Martinez et al. 1995). We calculate the primary gamma-ray energies with the obtained energy estimator and the number of electrons in showers boosted in the AEF of different strengths; see Table 2. The used estimator reproduces the energy used in the simulation very well (second column). However, when we use the shower sizes (N_e) boosted in AEF, the overestimation of the energy is drastic.

4. Discussion and Conclusions

Table 2 shows that 10 TeV primary gamma rays can already be attributed to the UHE domain. Showers from 100 TeV

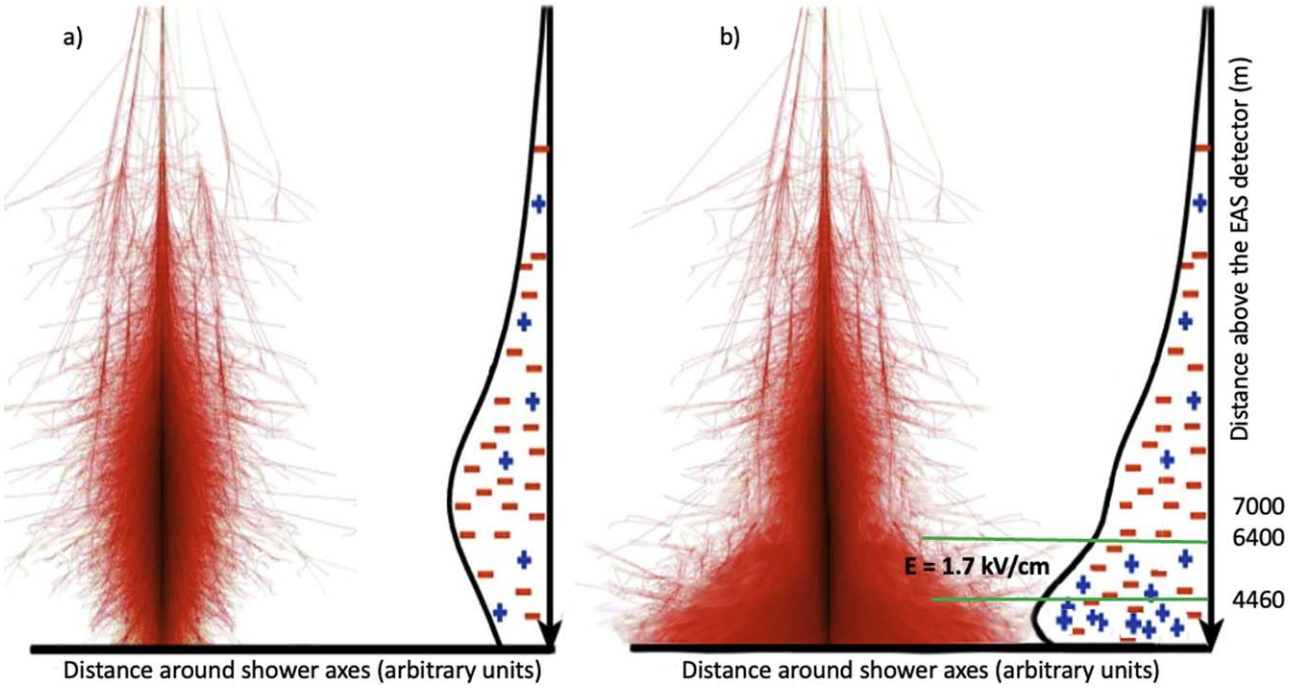

Figure 3. EAS propagation in the AEF during fair weather (a) and thunderstorm (b).

primaries can get a huge boost leasing to energies above PeV. Figure 3 illustrates what happens with EAS particles in the strong AEF. Figure 3(a) shows EAS development in fair weather and Figure 3(b) after electron multiplying in the AEF.

Numerous theoretical papers based on UHE gamma-ray observations discuss the origin of the Galactic PeVatron, gamma-ray propagation in the galaxy, and the possibilities of their registration (see, for instance, T. Sudoh & J. F. Beacom 2023; J. Zhang & Y. Guo 2024). Phenomenological models combining leptonic and hadronic fluxes from several galactic sources are developed to explain registered gamma rays in the energy range 10 GeV–10 TeV and 10 TeV–1 PeV consequently (see, for instance, A. De Sarkar & N. Gupta 2022). While several classes of stellar objects in the Milky Way seem able to accelerate hadrons to many tens of TeV energies, it remains mysterious which ones can reach PeV energies. If the gamma-ray sources are hadronic cosmic-ray accelerators, along with gamma rays, they should emit neutrino fluxes due to the pion-producing CR interactions with source matter. However, no neutrino sources have been detected.

From 1441 days of LHAASO operation to collect data for the first catalog, 33% of days were during the most frequent thunderstorms (from May to August). Thus, a precise consideration of climatic conditions is necessary to confirm the PeVatron detection, which is the most intriguing discovery in CR physics nowadays.

Appendix

The supplementary materials: the keyword input file for a CORSIKA run used in simulations of EAS propagation in the AEF above the LHAASO observatory.

CORSIKA code is available for downloading from https://web.iap.kit.edu/corsika/download/

RUNNR	1	run number
EVTNR	1	number of first shower event
NSHOW	1000	number of showers to generate
PRMPAR	1	particle type of prim. particle
ESLOPE	−2.7 slope of primary energy spectrum	
ERANGE	100.0E+3 100.0E+3	energy range of primary particle
THETAP	0. 0.	range of zenith angle (degree)
PHIP	−180. +180.	range of azimuth angle (degree)
SEED	1 0 0	seed for 1. random number sequence
SEED 2	0 0	seed for 2. random number sequence
FIXCHI	0	starting altitude (in g cm^{-2})
OBSLEV	441000.	observation level (in cm)
MAGNET	34.6 35.9	magnetic field LHAASO
HADFLG	0 0 0 0 0 2	flags hadr. interact. and fragmentation
ECUTS	0.3 0.3 0.003 0.003	energy cuts for particles
ELMFLG	F T	em. interaction flags (NKG,EGS)
STEPFC	1.	mult. scattering step length fact.
RADNKG	200.E2	outer radius for NKG lat.dens.distr.
ARRANG	0.	rotation of array to north
ECTMAP	1.E3	cut on gamma factor for printout
MAXPRT	1	max. number of printed events
DIRECT	/home/mary/results/	output directory
DATBAS	T	write .dbase file
USER	mary	user
DEBUG	F 6 F 1000000	debug flag and log.unit for out
EXIT	...	terminates input

ORCID iDs

A. Chilingarian https://orcid.org/0000-0002-2018-9715

References

Aharonian, F., Akhperjanian, A. G., Barrio, J. A., et al. 1999, PhRvD, 59, 092003
Albert, A., Alfaro, R., Alvarez, C., et al. 2024, ApJL, 973, L34
Amenomori, M., Bao, Y. W., Bi, X. J., et al. 2019, PhRvL, 123, 051101
Antoni, T., Apel, W., Badea, F., et al. 2002, APh, 662, 892

Antoni, T., Apel, W., Badea, F., et al. 2003a, NIMPA, 513, 490
Antoni, T., Apel, W., Badea, F., et al. 2003b, APh, 19, 715
Axikegu, X.-X., , Z., & Yun-Feng, Z. 2024, AcPSn, 73, 129201
Bass, S. 1998, PrPNP, 41, 225
Cao, Z., Aharonian, F., Axikegu, F., et al. 2024a, PhRvL, 132, 131002
Cao, Z., Aharonian, F., An, Q., et al. 2024b, ApJS, 271, 25
Chilingarian, A. A. 1989, CoPhC, 54, 381
Chilingarian, A., Daryan, A., Arakelyan, K., et al. 2010, PhRvD, 82, 043009
Chilingarian, A., Gharagyozyan, G., Ghazaryan, S., et al. 2007, APh, 28, 58
Chilingarian, A., Gharagyozyan, G., Hovsepyan, G., et al. 2004, ApJL, 603, L29
Chilingarian, A, Hovsepyan, G, & Zazyan, M 2022, JPhCS, 2398, 012001
Chilingarian, A., & Mkrtchyan, H. 2012, PhRvD, 86, 072003
Chilingarian, A., Sargsyan, B., Karapetyan, T., et al. 2024, PhRvD, 110, 063043
Chilingarian, A., & Zazyan, H. 1991, NCimC, 14, 555
De Sarkar, A., & Gupta, N. 2022, ApJ, 934, 118
Du, Y., Zheng, D., Ma, R., et al. 2022, RemS, 14, 2855
Fan, P., Zheng, D., Zhang, Y., et al. 2018, JAtOT, 35, 927
Gurevich, A. V., Milikh, G. M., & Roussel-Dupre, R. A. 1992, PhLA, 165, 463
Heck, D., Knapp, J., Capdeville, J. N., et al. 1998, CORSIKA: A Monte Carlo Code to Simulate Extensive Air Showers (Karlsruhe: Forschungszentrum Karlsruhe GmbH)
Heck, D., & Pierog, T. 2024, Extensive Air Shower Simulation with CORSIKA: A User's Guide (Eggenstein-Leopoldshafen: Institut für Astroteilchenphysik, Karlsruher Institut für Technologie (KIT))
Hovsepyan, G., & Chilingarian, A. 2023, BRASP, 87, 1039
Kalmykov, N. N., Ostapchenko, S. S., & Pavlov, A. I. 1997, NuPhS, 52, 17
Kulikov, G. V., & Christiansen, G. B. 1958, JETP, 35, 441
Kuettner, J 1950, JAtS, 7, 322
Lin, C., Xun-xiu, Z., Axikegu, C., et al. 2024, ChA&A, 48, 263
Liu, D., Li, F., Qie, X., et al. 2024, GeoRL, 51, e2024GL109602
Ma, R., Zheng, D., Yao, W., & Zhang, W. 2021, JApMC, 32, 358
Martinez, S., Arqueros, F., Fonseca, V., et al. 1995, NIMPA, 357, 567
Nelson, W. R., Hirayama, H., & Rogers, D. W. O. 1985, The EGS4 Code System ReportSLAC, Stanford Linear Accelerator Center 265
Qie, X., Zhang, T., Zhang, G., Zhang, T., & Kong, X. 2009, AtmRe, 91, 244
Sudoh, T., & Beacom, J. F. 2023, PhRvD, 107, 043002
Williams, E., Mailyan, B., Karapetyan, G., & Mkrtchyan, H. 2023, JGRD, 128, e2023JD039612
Zhang, J., & Guo, Y. 2024, arXiv:2409.00477
Zhu, J., Zhi, S., & Ren, S. 2023, Atmos, 14, 1765
Zou, T., Zhang, Q., Li, W., & Li, J. 2018, GeoRL, 45, 4485